Bioactive Materials 26 (2023) 159–168

Contents lists available at ScienceDirect

Bioactive Materials

journal homepage: www.keaipublishing.com/en/journals/bioactive-materials

Stem cell niche-inspired microcarriers with ADSCs encapsulation for diabetic wound treatment

Xiangyi Wu [a], Haofang Zhu [a], Junyi Che [a], Ye Xu [a,**], Qian Tan [a,***], Yuanjin Zhao [a,b,*]

[a] Department of Burns and Plastic Surgery, Institute of Translational Medicine, The Affiliated Drum Tower Hospital of Nanjing University Medical School, Nanjing, 210002, China

[b] Oujiang Laboratory (Zhejiang Lab for Regenerative Medicine, Vision and Brain Health), Wenzhou Institute, University of Chinese Academy of Sciences, Wenzhou, Zhejiang, 325000, China

ARTICLE INFO

Keywords:
Stem cell
Bio-inspired
Microfluidics
Microcarrier
Wound healing
Hydrogel

ABSTRACT

Stem cell therapies have made great progress in the treatment of diabetic wounds during recent decades, while their short in vivo residence, alloimmune reactions, undesired behaviors, and dramatic losses of cell functions still hinder the translation of them into clinic. Here, inspired by the natural components of stem cell niches, we presented novel microfluidic hydrogel microcarriers with extracellular matrix (ECM)-like composition and adipose-derived stem cells (ADSCs) encapsulation for diabetic wound healing. As the hydrogel was synthesized by conjugating hyaluronic acid methacryloyl (HAMA) onto the Fibronectin (FN) molecule chain (FN-HAMA), the laden ADSCs in the microcarriers showed improved bioactivities and pro-regenerative capabilities. Based on these features, we have demonstrated that these ADSCs microcarriers exhibited significant promotion of neovascularization, follicular rejuvenation, and collagen deposition in a mouse diabetic wound model. These results indicated that the stem cell niche-inspired FN-HAMA microcarriers with ADSCs encapsulation have great clinical potential for diabetic wound treatment.

1. Introduction

Diabetic wound is characterized by delayed wound healing and the persistence of their therapeutic impediments [1–3], which poses an economic and medical burden worldwide. Long-lasting diabetic wounds are prone to infection, leading to severe sepsis or septicemia, causing amputation and even death as adverse outcomes [4–6]. Current strategies like debridement, decompression, and revascularization remain suboptimal, as evidenced by poor therapeutic effects and high recurrence rates [7–9]. As an alternative stratagem, stem cells, especially adipose-derived stem cells (ADSCs), have gained significant attention due to their strong differentiation potential and paracrine activities [10–12]. Thus, the ADSCs therapies show promise to ameliorate diabetic wound healing [13,14]. Although with many successes, most of these therapies are through direct ADSCs administration, which usually leads to alloimmune reactions, undesired behaviors, and dramatic losses of cell functions [15,16]. To overcome these limitations, hydrogel encapsulation has become an attractive approach [17–20] and diverse hydrogel scaffolds have been developed for stem cell delivery [21,22]. However, these bulk hydrogel delivery systems are usually suffering from poor gas permeability and inefficient diffusion of biomolecules due to their large volume, which commonly induces inferior cell viability and limited therapeutic efficacy [23–25]. Therefore, new ADSCs carriers with increased diffusional transport, improved in vivo cell persistence and fitness are still anticipated [26].

Here, inspired by natural stem cell niches, we proposed novel microfluidic microcarriers with extracellular matrix (ECM)-like composition and ADSCs encapsulation for diabetic wound healing. ECM components within the stem cell niches, such as structural and functional protein, are essential for the modulation of cell characteristics and maintenance of cell bioactivity [27–29]. As one of the main ECM protein, fibronectin (FN) have demonstrated its unique effects in

Peer review under responsibility of KeAi Communications Co., Ltd.

* Corresponding author. Department of Burns and Plastic Surgery, Institute of Translational Medicine, The Affiliated Drum Tower Hospital of Nanjing University Medical School, Nanjing, 210002, China.

** Corresponding author.

*** Corresponding author.

E-mail addresses: wuxiangyi@smail.nju.edu.cn (X. Wu), 1024613582@qq.com (Y. Xu), smmutanqian@sina.com (Q. Tan), yjzhao@seu.edu.cn (Y. Zhao).

https://doi.org/10.1016/j.bioactmat.2023.02.031

Received 20 September 2022; Received in revised form 26 January 2023; Accepted 27 February 2023

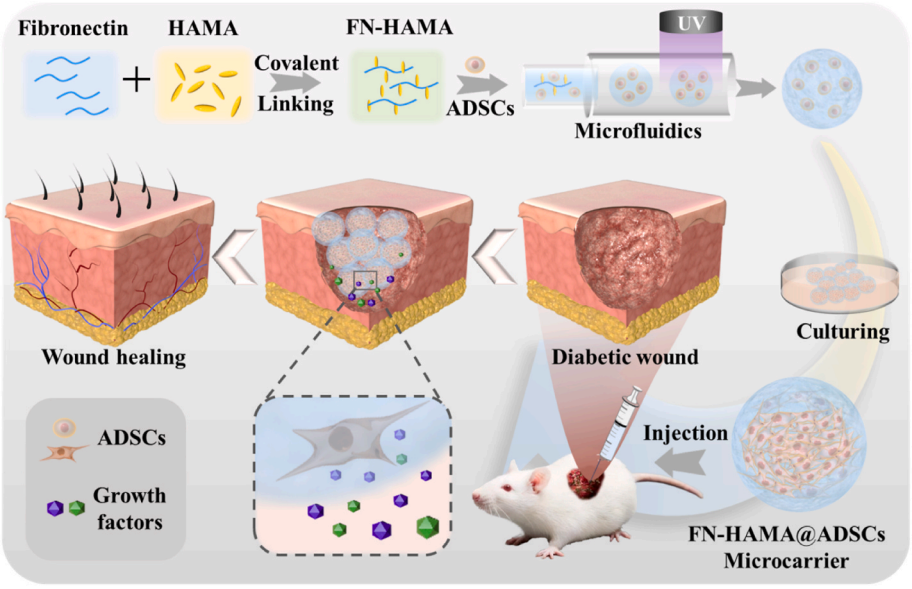

Fig. 1. Schematic of the fabrication of FN-HAMA microcarriers with ADSCs encapsulation and their application in promoting diabetic wound healing.

modulating mechanotransduction events, which could significantly influence the behavior (e.g., morphology, adhesion, differentiation) of stem cells [30–32]. In addition, FN could be tailored to various polymers for enhancing cell adhension on hydrogel materials [33]. Generally, droplet microfluidic technology allows for the fabrication of monodisperse hydrogel microcarriers with precisely tunable sizes and large surface area [34–37]. The resultant microcarriers enable the microencapsulation of stem cells and supply a much biocompatible environment for their survival, proliferation, and differentiation [38,39]. Thus, it is conceivable that the combination of FN-engineered microcarriers and microfluidics-based cell encapsulation would offer exciting possibilities for stem cell niches reconstruction and provide an unprecedented strategy to solve existing difficulties in clinical ADSCs therapies. To our knowledge, although FN-modified polymers have been broadly engaged in biomedicine [40–43], research on the treatment of diabetic wound healing with the stem cell niche-mimicking ADSCs microcarriers has never been reported.

In this study, by conjugating hyaluronic acid methacryloyl (HAMA) onto the FN molecule chain (FN-HAMA), we fabricate the desired photocurable microcarriers with therapeutic ADSCs encapsulation (FN-HAMA@ADSCs) for the hard-healing diabetic wounds regeneration (Fig. 1). These microcarriers with mono-dispersity and injectability were fabricated by using microfluidic emulsification technology. Due to the incorporation of FN, the hydrogel components of the microcarriers were imparted with good cell adhesion and cytocompatibility. Thus, an optimal pre-culture of the engineered ADSCs microcarriers allowed for improved pro-regenerative capabilities and enhanced biomass production, which eventually provided better in vivo outcomes. Importantly, it was demonstrated that these ADSCs microcarriers exhibited significant promotion of neovascularization, follicular rejuvenation, and collagen deposition in a mouse diabetic wound model, suggesting desirable wound repair. These distinguishing features indicated that the FN-HAMA microcarriers could bring significant value to stem cell therapies for clinical diabetic wound healing.

2. Methods

2.1. Synthesis and characterization of HAMA

Briefly, hyaluronic acid (Mw:10 kDa1.0 MDa, Bloomage Biotechnology) (4 g) was dissolved in phosphate-buffered saline (PBS) (Invitrogen) (200 mL) at room temperature using a magnetic stirrer. To the HA solution, 15 mL of methacrylic anhydride (Sigma) was slowly added dropwise, stirred vigorously at 0 °C for 24 h, and the pH was conditioned with 1 M NaOH (Aladdin) solution and maintained between 8 and 9. The solution was then dialyzed with a 12–14 kDa membrane for one week to remove unreacted methacrylic anhydride. Finally, the dialysis-completed HAMA solution was lyophilized.

The extent of methacrylation was determined using 1H NMR (Varian Inova 500). The characteristic peak of the methacrylamide moiety of hyaluronic acid was located. The degree of methacrylation was derived by calculating the ratio of the number of reacted methacrylamide groups to the number of unreacted amine groups in the hyaluronic acid.

2.2. Synthesis of FN-HAMA

Firstly, HAMA was dissolved in PBS at a concentration of 5% (w/v) and stirred at room temperature until completely dissolved. To obtain FN-HAMA with 25%, 50% and 75% grafting ratio, equimolar amounts of NHS (Sigma) with EDC (Sigma) were added to the solution at 0.25 mM, 0.50 mM and 0.75 mM, respectively, and stirred for 30 min at room temperature. Next, fibronectin (Med Chem Express) was added at a concentration of 50 μg/ml and the solution was stirred at room temperature overnight. Finally, the solution was lyophilized and placed at −80 °C for further use. Then the molecular mass of the FN-HAMA with different grafting ratios were measured by gel permeation chromatography (*GPC*).

2.3. FN persistence

To examine FN persistence time, composite hydrogels fabricated through physical mixing and covalent grafting were made into uniformly sized blocks and placed in 6-well plates. 5 wt% HAMA solution with fibronectin (50 μg/ml) was used in the physical mixing group, and 5 wt% FN-HAMA (75% grafting ratio) solution was used in the covalent grafting group. The solution in the supernatant was collected after 24, 48, 72, and 96 h of incubation in PBS to assess the retention of FN. Quantification was performed using the bicinchoninic acid colorimetric assay (MicroBCA Assay Kit, Beyotime Biotechnology). Briefly, standards and samples mixed with working reagents are loaded into a 96-well microplate. The microtiter plate was then sealed and incubated for 2 h at 37 °C. Following incubation, the microtiter plate was allowed to cool at RT for 20 min, protected from light. Measure the absorbance at 562 nm using a plate reader (BIOTEK).

2.4. Culture of ADSCs

ADSCs (Catalog #7510, ScienCell) isolated from human adipose tissue were used in this study. α-Minimal Essential Medium (MEM) supplemented with 10% FBS, 100 U/mL penicillin G, and 100 mg/mL streptomycin (Procell) were used for cell culture. The medium was replaced every 2–3 days. Cells of 4–6 generations were used in the experiments.

2.5. Cell adhesion in FN-HAMA

5% (w/v) FN-HAMA containing 1% (w/v) HMPP (Sigma) was added to the disc and cured under UV light and FN-HAMA hydrogel was formed (5 mm thick, 3 cm length). After being lyophilized, the hydrogel films were plated in a 6-well plate. GFP-labeled ADSCs were then inoculated onto the hydrogel films at a density of 4×10^5/ml. After 48 h, the hydrogel films were washed with PBS and the adhered cells were observed by CLSM.

2.6. Fabrication and characterization of FN-HAMA microcarriers

FN-HAMA microcarriers were fabricated through using a microfluidic device consisting of one square glass and two circular capillaries arranged on a glass slide. The diameters of the inner and outer capillaries were 580 μm and 1 mm, respectively. After being tapered with a micropipette puller (Sutter Instrument), the inner capillarity was polished to achieve an diameter of approximately 200 μm. These round capillaries for internal phase input and final emulsion collection were assembled coaxially in a 1-mm inner diameter square capillary tube (AIT Glass). All equipment connections are epoxy sealed. Pregel solution containing 1% HMPP (w/v) and 5% FN-HAMA (w/v) were configured as the inner phase. Paraffin containing 5% span 80 was configured as the outer phase. A glass syringe (SGE Analytical Science) was used to inject each fluid into the microfluidic device through polyethylene tubing (Scientific Commodities Inc.) and a syringe pump (Harvard PHD 2000 Series) was used for pumping. To obtain a suitable microcapsule size, the flow rate of the oil phase was kept at 50 μm/min, while the water phase was regulated from 1 μm/min to 10 μm/min. The flow rate ratio varied from 0.02 to 0.1 and the diameter of the microspheres varied from 150 μm to 280 μm. The droplets were solidified under UV light (365 nm, 7 w) for 20 s and collected with paraffin, and the formed FN-HAMA microcarriers are washed by centrifugation to remove the excess paraffin. The inverted microscope (AE2000, Motic) was used to observed the real-time images of the fabrication process. AOS Imaging Studio V3.4.2 software was used to measure the diameter of FN-HAMA microcarriers.

To further observe the distribution of FN in FN-HAMA microcarriers, FN-HAMA was prepared with Alexa Fluor 750-labeled FN. The labeling procedure was performed according to the instructions. Briefly, FN-HAMA was dissolved PBS (5%, w/v) and Alexa Fluor™ 750 NHS Ester (0.1%, v/v, Invitrogen) was added. The FN-HAMA solution was stirred overnight at room temperature. Microcarriers were prepared using Alexa Fluor 750-labeled FN-HAMA and observed under CLSM.

2.7. Physical characterization of the FN-HAMA microcarriers

In vitro degradation of FN-HAMA microcarriers was evaluated using enzyme-promoted degradation. 500 μL of the samples were incubated at 37 °C with 500 μL of DPBS containing 20 U/mL of hyaluronidase in 1.5 mL Eppendorf tubes for 16 days. Hyaluronidase-containing DPBS was replaced every day to ensure constant enzymatic activity. At predetermined time points, the DPBS was removed from tubes. Then, the samples were washed twice with sterile deionized (DI) water, lyophilized, and weighed. Degradation rate (%) $= (W_0 - W_t)/W_0 \times 100\%$.

For swelling characterization, the FN-HAMA microcarriers were lyophilized to obtain their dry weight (Wd). These samples were separately immersed in DI water, and their weights were monitored daily until the equilibrium swelling weight (Weq) was obtained. The experiments were performed in triplicate under the same conditions. The swelling ratio (%) $=$ Weq/Wd $\times$ 100%.

2.8. In vitro biological effects of FN-HAMA microcarriers

2.8.1. Encapsulation of the ADSCs

Cell suspensions containing 1% HMPP (w/v), 5% FN-HAMA (w/v), and 10^6/ml ADSCs were configured as the inner phase. Paraffin containing 5% span 80 was configured as the outer phase. The flow rate of the oil phase was kept at 50 μm/min, and the water phase was kept at 5 μm/min. The solidification and washing steps are the same as in 2.6.

2.8.2. Cell viability

To monitor the viability of cells encapsulated in microcarriers, the live-dead assay was performed using a commercially available kit (Beyotime). Briefly, FN-HAMA@ADSCs were cultured for 3, 7, and 14 days and then seeded at a concentration of 100 microcarriers/well on 6-well plates. The staining working solution was configured with 0.1% (v/v) Calcein AM and 0.1% (v/v) propidium iodide and was added 1 ml to each well. After incubation for 30 min at 37 °C, the FN-HAMA@ADSCs were observed by fluorescence microscopy. HAMA@ADSCs and FN/HAMA@ADSCs were set as control. Cell viability was quantified by calculating the proportion of live cell fluorescence intensity using Image J. Cell proliferation was quantified with live cell fluorescence intensity normalized to the total cell fluorescence intensity on day 3 of the HAMA@ADSCs group.

2.8.3. Cell stemness

To assess the effect of FN-HAMA microcarriers on cell stemness maintenance, flow cytometric assays were performed to test cell surface markers expression. After two weeks of culture, ADSCs released from the microcarriers were collected and incubated with the antibodies of CD105, CD90, CD73, CD45, and CD34. The flow cytometric analysis was conducted with BD FACSCalibur flow cytometer (BD Biosciences). The data was analyzed with FlowJo version 10. Cells with CD105, CD90, CD73 positivity above 95% and CD45, CD34 positivity below 5% were considered to possess stemness.

2.8.4. Angiogenic potential

To evaluate the pro-angiogenic capacity of the FN-HAMA@ADSCs, HUVEC cells were used for in vitro tube formation assays. Then 100 μL per well of Matrigel was added to a 48-well plate and incubated at 37 °C for 30 min before seeding the cells. The supernatants of each group were prepared as follows: For the ADSCs group, the culture supernatants of 1×10^6 cells with 72 h of monolayer culture were collected. For the microcarrier groups, microcarriers loaded with 1×10^6 ADSCs were incubated for 72 h and their culture supernatants were collected by centrifugation at 100×*g* for 5 min. Each well was seeded with 2×10^4 HUVEC cells and cultured with 500 μL supernatants of ADSCs, HAMA@ADSCs, FN/HAMA@ADSC and FN-HAMA@ADSCs, respectively. After 24 h, HUVEC cells were labeled with Calcein AM and tube formation on each well was examined under CLSM. The total tube length, number of meshes and number of junctions were analyzed by the ImageJ.

2.8.5. Gene expression

qPCR assays were performed to examine the expression level of HIF-1, FGF2, VEGF, and Ang-1 by ADSCs loaded in the microcarriers. We used SteadyPure Universal RNA Extraction Kit (Accurate Biology) to extract RNA from HAMA@ADSCs, FN/HAMA@ADSC and FN-HAMA@ADSCs. The Evo M-MLV RT Kit (Accurate Biology) was used for reverse transcription to reverse transcribe RNA to cDNA. Gene expression of HIF-1, FGF2, VEGF, and Ang-1 were determined by quantification. Real-time polymerase chain reaction analysis (qRT-PCR, QuantStudio 7 Pro systems, Invitrogen, USA) with gene primers. The

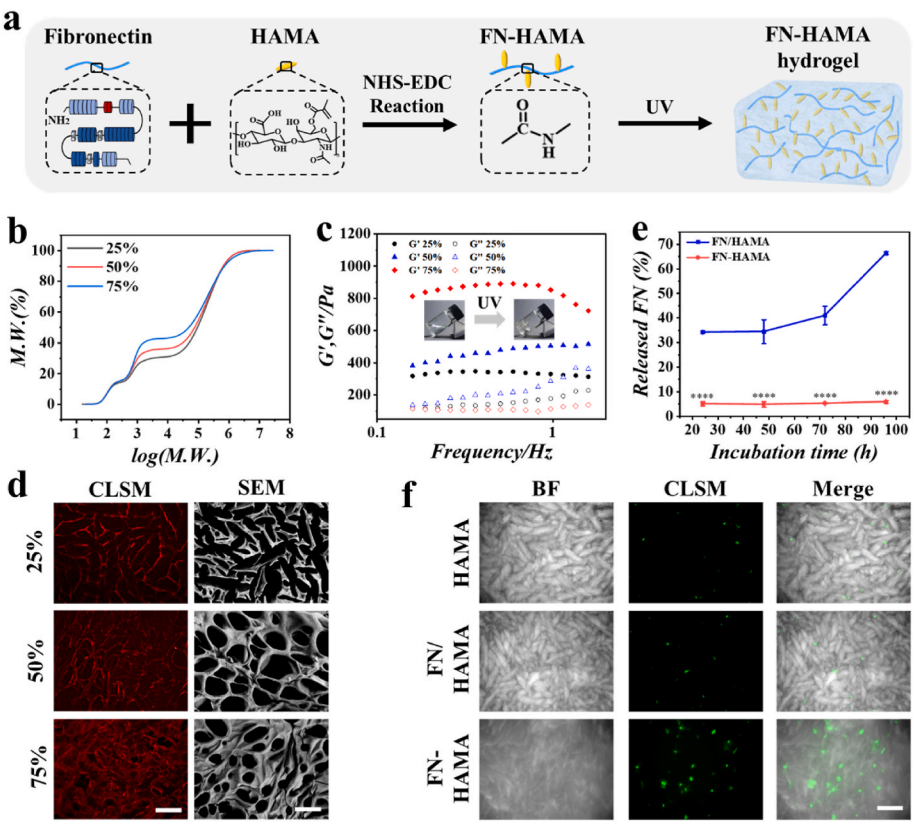

Fig. 2. Fabrication and characterization of the FN-HAMA hydrogel. (a) The synthesis of FN-HAMA pre-polymer and the fabrication of FN-HAMA hydrogels. (b) GPC of FN-HAMA with different graft ratios. (c) Frequency sweep of the FN-HAMA hydrogel with 75% graft ratio. (d) CLSM images (Scale bar: 100 μm) and SEM images of FN-HAMA hydrogels with different graft ratios. (e) Release kinetics of FN within 96 h from FN-HAMA and FN/HAMA hydrogels, respectively. (f) Representative bright-field and fluorescent photographs of adherent GFP-labeled ADSCs in HAMA, FN/HAMA, and FN-HAMA hydrogels after 48 h of incubation. Scale bar:100 μm *$p < 0.05$, **$p < 0.01$, ***$p < 0.001$, ****$p < 0.0001$, not significant (ns).

relative gene expression levels of ADSCs were obtained accordingly by normalizing the internal control β-actin. Primer sequences are listed below (F: forward, R: reverse primer). HIF-1 F 5′-GAACGTCGAAAAGAAAAGTCTCG-3′; HIF-1 R 5′-CCTTATCAAGATGCGAACTCACA-3′; FGF2 F 5′-AGAAGAGCGACCCTCACATCA-3’; FGF2 R 5′-CGGTTAGCACACACTCCTTTG-3’; VEGF F 5′-AGGGCAGAATCATCACGAAGT-3’; VEGF G 5′-AGGGTCTCGATTGGATGGCA-3’; Ang-1 F 5′-CTGGGCGTTTTGTTGTTGGTC-3’; Ang-1 R 5′- GGTTTGGCATCATAGTGCTGG-3’; GAPDH F 5′- GGAGCGAGATCCCTCCAAAAT-3’; R 5′-GGCTGTTGTCATACTTCTCATGG -3’.

2.8.6. Growth factor secretion

ELISA was performed to verify the secretion of VEGF, HGF, and FGF2 by ADSCs laden in HAMA, FN/HAMA or FN-HAMA microcarriers by collecting the supernatant of microcarriers cultured for 7 days. ELISA assays were performed with Human Insulin ELISA Kit (Elabscience) according to the instructions.

2.9. In vivo evaluation of FN-HAMA microcarriers

2.9.1. Wound healing evaluation

For in vivo experiment, 1 ml of FN/HAMA@ADSCs and 1 ml of FN-HAMA@ADSCs containing 1×10^6 ADSCs were fabricated and incubated for one week. The unloaded FN-HAMA microcarriers with equal volume were also prepared. At the same time, 1×10^6 ADSCs were seeded and cultured for one week. The unloaded FN-HAMA microcarriers, FN/HAMA@ADSCs, FN-HAMA@ADSCs, and ADSCs were resuspended with 1 mL PBS, respectively. To establish type I diabetic mice, streptozotocin (100 mg/kg) was injected intraperitoneally into male Balb/c mice (aged 6–8 weeks, weighed~20 g) after 24 h of fasting. 1 week later, the blood glucose of each mouse was confirmed. To induce diabetic wounds, the back of each mouse was shaved and two circular full-thickness skin wounds of 8 mm in diameter were created on both sides of the spine. After being divided into five groups (three mice per group), the mice were treated with PBS, ADSCs, FN-HAMA, FN/HAMA@ADSCs and FN-HAMA@ADSCs. 500 μL of the PBS, cell suspension, and microcarrier suspension were injected around the wound edges, perspectivity. The wound area was recorded daily. On day 9, the remaining wound tissue was collected, sectioned, and subjected to immunofluorescence staining (CD 31) and histological staining (H&E or Mason staining).

2.9.2. Cell distribution

In addition, to evaluate the cell distribution in vivo, we conducted cell tracking experiments using the in vivo image system. Firstly, ADSCs were transduced with a recombinant retroviral vector expressing the *mCherry* fluorophore. After that, the *mCherry*-labeled ADSCs were loaded into microcarriers as described above. The mice were divided into three groups (three mice for each group) after modeling and received the treatment of *mCherry*-labeled ADSCs, FN/HAMA@*mCherry*-labeled ADSCs, and FN-HAMA@ *mCherry*-labeled ADSCs. Mice were imaged with the in vivo imaging system (IVIS System, PerkinElmer) immediately (0 h) and 72 h after treatment, respectively.

2.9.3. In vivo biocompatibility studies

Major organs were also harvested and subjected to H&E staining to detect the toxicity of the applied material. All animal experiments were approved by the Animal Investigation Ethics Committee of Nanjing Drum Tower Hospital and performed in accordance with ethical guidelines. The approval number issued by the Laboratory Animal Welfare Ethics Committee of Drum Tower Hospital was 2020AE01109.

2.10. Statistical analysis

All experiments described above were repeated three times. The experimental data were presented as mean ± standard error of the mean. Student's *t*-test, one-way ANOVA and two-way ANOVA were used to conduct the statistical analysis with Origin 8. Differences were

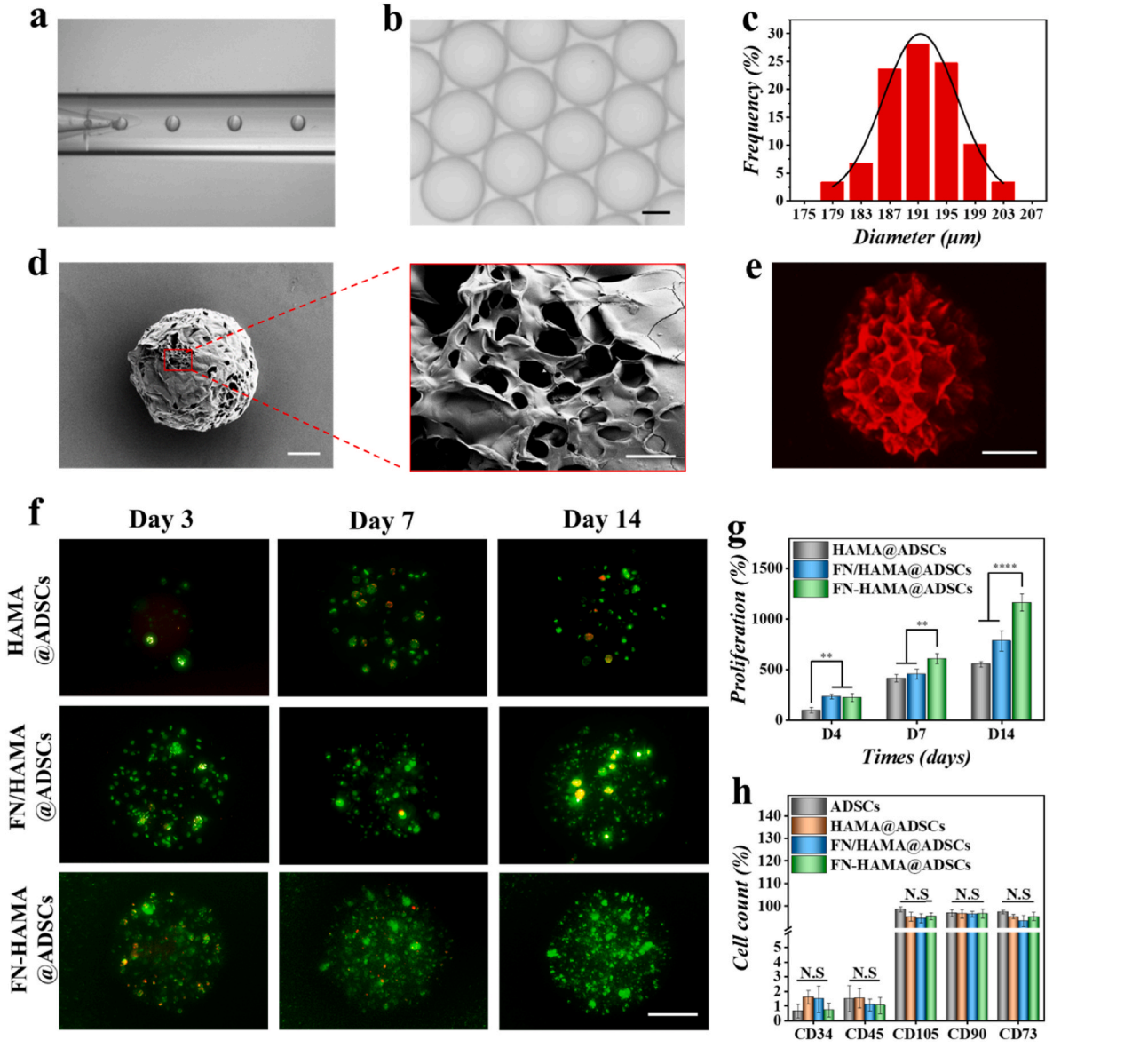

Fig. 3. Fabrication and characterization of FN-HAMA@ADSCs. (a) Microscope image of the FN-HAMA droplets generated in the microfluidic device. (b) Bright-field image of monodisperse FN-HAMA droplets. Scale bar: 100 μm. (c) Particle size distribution of the FN-HAMA microcarriers. (d) SEM images of the whole view (Scale bar: 50 μm) and the enlarged view (Scale bar: 50 μm) of FN-HAMA microcarriers. (e) CLSM image of Alexa 750 labeled FN-HAMA microcarriers. Scale bar: 50 μm. (f) Representative fluorescent photographs of ADSCs laden in the FN-HAMA microcarriers on days 3, 7, and 14. Live and dead cells were labeled with Calcein AM and propidium iodide. Scale bar: 100 μm. (g) Quantification of cell proliferation of laden ADSCs. (h) Quantification of the flow cytometric results. *$p < 0.05$, **$p < 0.01$, ***$p < 0.001$, ****$p < 0.0001$, not significant (ns).

considered statistically significant at p-values less than 0.05 and statistical differences were considered at *$p < 0.05$, **$p < 0.01$, ***$p < 0.001$, ****$p < 0.0001$, not significant (ns), and $p > 0.05$.

3. Results and discussion

3.1. Synthesis and characterization of FN-HAMA

HAMA was synthesized according to conventional procedures. The degree of substitution of methacryloyl was detected as 75% by 1H nuclear magnetic resonance spectroscopy (1H NMR) (Fig. S1). Then, the synthetic HAMA was conjugated to FN backbone by N-Hydroxysuccinimide/1-ethyl-3-(3-dimethylaminopropyl)-carbodiimide NHS/EDC) coupling chemistry, enabling the promotion of cell adhesion and cytocompatibility of the resultant FN-HAMA hydrogels (Fig. 2a). The FN-HAMA monomer with different graft ratio (25%, 50%, and 75%) were characterized by gel permeation chromatography (GPC) (Fig. 2b). FN-HAMA hydrogels were then fabricated with a photo-initiator under UV light (inset picture of Fig. 2c). The formed FN-HAMA hydrogel showed a storage modulus (G′) constantly larger than the loss modulus (G″), typical behavior of a hydrogel network, ensuring a stable physiological environment for loaded ADSCs (Fig. 2c). The excellent resistance to deformation possessed by FN-HAMA can maintain the biological activity of encapsulated cells for the treatment of diseases.

To further understand FN-HAMA hydrogels' porosity and internal morphology, we observed the vacuum-dried microgels under scanning electron microscopy (SEM) and confocal laser scanning microscopy (CLSM). FN-HAMA hydrogels with different graft ratios exhibited highly uniform porous structures (Fig. 2e). As the graft ratio increased, a denser network was obtained, which is vital for providing mechanical support to cell growth. Thus, FN-HAMA hydrogel with a 75% grafting ratio was chosen for further study.

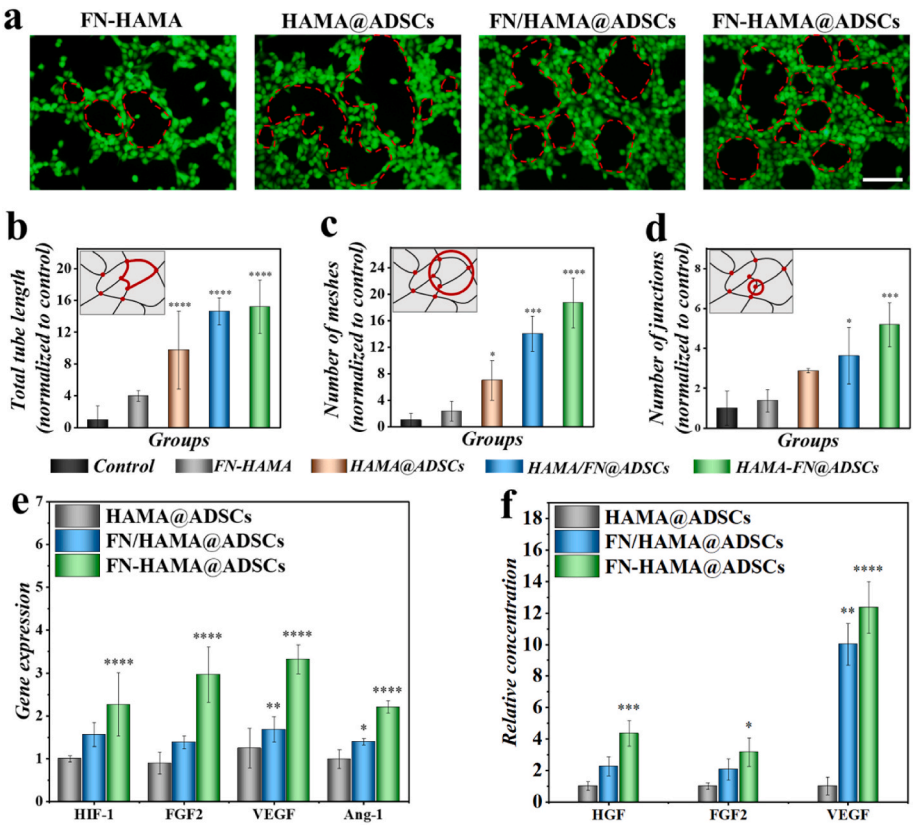

Fig. 4. Pro-angiogenesis of FN-HAMA@ADSCs. (a) Representative fluorescent images of the tubule network structure of HUVEC after co-culture with ADSCs and different microcarriers. Scale bars:100 μm. (b, c, d) Quantitative assessment of the formed tubule. (e) Normalized gene expression levels of encapsulated ADSCs in microcarriers. (f) Levels of growth factors released from microcarriers as quantified by ELISA. *p < 0.05, **p < 0.01, ***p < 0.001, ****p < 0.0001, not significant (ns).

As a significant functional protein in the ECM, FN has been considered a major regulatory component affecting cell adhesion ability and bioactivity, and stable maintenance is essential for fibronectin to function effectively [27]. Therefore, we examined the persistence time of FN in FN-HAMA hydrogels, HAMA hydrogels with physically incorporated FN (FN/HAMA) were used as control. At 96 h, a 70% release of FN was observed for FN/HAMA hydrogels, while FN-HAMA hydrogels with chemical conjugation only reached a loss of less than 5%, indicating prolonged and stable retention of functional FN molecules (Fig. 2d). Next, we detect the regulatory effect of FN-HAMA hydrogels on cell adhesion. As expected, the FN-HAMA hydrogels showed significantly promoted cell adhesion compared to HAMA hydrogels without the addition of FN as well as FN/HAMA hydrogels with the physical blend of FN (Fig. 2f, S2). This phenomenon should be attributed to the superior adhesive support of FN on cells, which corroborates previous studies that highlighted the significant role of fibronectin in modulating cell regenerative capabilities [27,44].

3.2. Microfluidic fabrication of FN-HAMA microcarriers

Currently, mesenchymal stem cells (MSCs) are attractive in biomedicine because of their regenerative and immunomodulatory functions. Here, ADSCs were loaded within FN-HAMA microgels for the treatment of diabetic wounds. In a typical experiment, stem cell niche-inspired microcarriers were fabricated by an oil-in-water emulsion using the microfluidic device shown in Fig. S3. The aqueous phase consists of 5 wt% FN-HAMA prepolymer, and 1 wt% 2-hydroxy-2-methylpropiophenone (HMPP) was pumped into the internal capillary, and the oil phase consists of 5% Span80 in paraffin oil was pumped into the external capillary. As a result, FN-HAMA droplets were formed when the aqueous phase was sheared by the oil stream (Fig. 3a). The FN-HAMA droplets are monodispersed with a controllable diameter varied from 150 μm to 280 μm by tuning the flow velocities of aqueous and oil phases (Fig. S4). To ensure sufficient encapsulated cells and surface contact area, droplets with a diameter of 200 μm were chosen for further studies (Fig. 3b and c).

3.3. Morphology and degradation behavior of FN-HAMA microcarriers

After lyophilization, the FN-HAMA microcarriers showed a spherical form with a porous structure using SEM analysis, allowing a satisfactory exchange of water and nutrients (Fig. 3d). In a swollen state, this interconnected porous architecture was also observed by CLSM using fluorescently labeled FN-HAMA prepolymers (Fig. 3e). Besides, FN-HAMA microcarriers displayed sufficient water retention capacity with a swelling ratio of 1100 wt% after incubation in deionized water, a prerequisite for the survival of encapsulated cells (Fig. S5). Meanwhile, the degradation of FN-HAMA microcarriers in a hyaluronidase solution (20 U/mL) was assessed. A gradual mass decrease was observed with increasing time and a 53% degradation was obtained by day 16 (Fig. S6), indicating the cell growth microenvironment provided by FN-HAMA microcarriers was maintained throughout the wound healing process. The degradation curve suggested that the hyaluronic acid would eventually be degraded, and the released stem cells may remain in the tissue and continue to play an immunomodulatory role to reduce scar formation.

3.4. Biocompatibility of FN-HAMA microcarriers

It is well known that the good biocompatibility of microcarriers is the primary prerequisite to ensuring the activity of the loaded cells. Both ADSCs cultured with HAMA, FN/HAMA, and FN-HAMA microcarrier extracts and released from the microcarriers after 2 weeks exhibited a typical spindle morphology, suggesting the excellent cytocompatibility of the microcarriers (Fig. S7). We further encapsulated the ADSCs into the stem cell niche-inspired FN-HAMA microcarriers (details are in "Methods") and demonstrated the cell proliferation and viability. Under optical microscope (OM) and CLSM observation, ADSCs exhibited

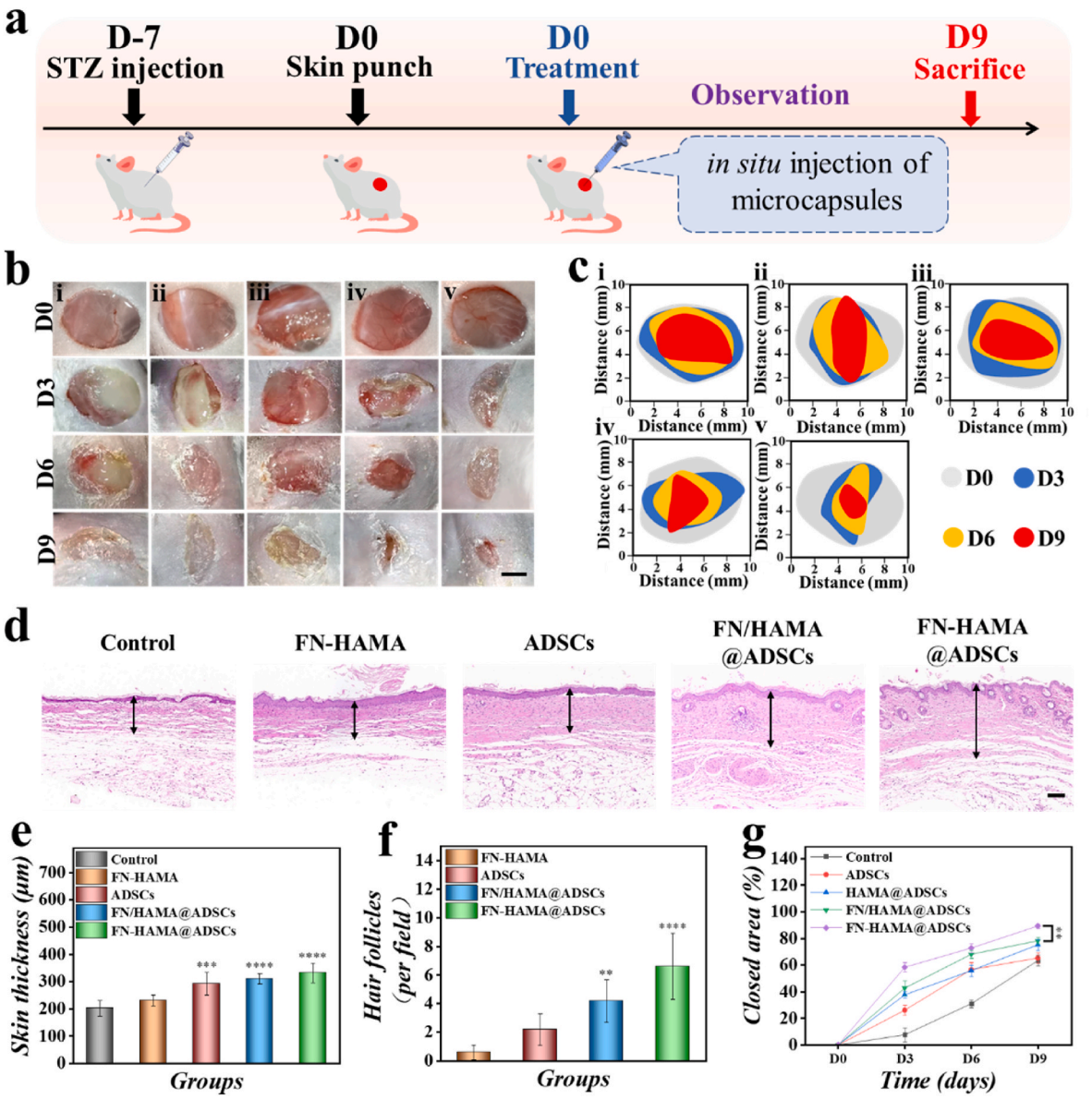

Fig. 5. In vivo diabetic wound healing evaluation of the FN-HAMA@ADSCs. (a) Schematic description of animal experiments. (b) Representative photos of diabetic wounds treated with PBS(i), FN-HAMA (ii), ADSCs(iii), FN/HAMA@ADSCs(iv), FN-HAMA@ADSCs(v) on day 0, 3, 6, and 9. Scale bar: 2 mm. (c) Wound area tracing analysis corresponding to photographs shown in Fig. 5b. (d) Representative images of H&E staining of the wound areas on Day 9. Scale bar:100 μm.(e) Statistical analysis of histological dermal thickness. (f) Statistical evaluation of the number of hair follicles. (g) Quantitative analysis of the wound areas. *$p < 0.05$, **$p < 0.01$, ***$p < 0.001$, ****$p < 0.0001$, not significant (ns).

significant proliferation and uniform distribution in the microcarriers, revealing a biocompatible micro-environment offered by FN-HAMA microcarriers (Fig. 3f, S8). In contrast, the fluorescence intensity of live cells in HAMA microgels was consistently lower than both FN/HAMA and FN-HAMA microcarrier groups during two weeks of culture. The fluorescent quantitative data were highly consistent with the CLSM results (Fig. 3g, S9). This favorable pro-proliferative effect should mainly be ascribed to the stem cell niches mimicking polysaccharide/peptide components of FN-HAMA microcarriers and the stable anchoring of FN as demonstrated above. Aside from cell viability, cell stemness has been demonstrated as another vital factor affecting therapeutic efficiency [45,46]. Cell stemness refers to the self-renewal ability and differentiation potential of stem cells. When stem cells were differentiated, their cell stemness and pro-regenerative functions, such as the secretion of various growth factors, were lost. Indeed, stabilization of cell stemness was *indispensable for any stem cell-based therapy*. Therefore, flow cytometry was conducted to evaluate the stemness of ADSCs in varied microcarriers. After 30 days of co-culture, the surface protein expression of ADSCs released from microcarriers showed no statistical difference compared with ADSCs seeded on tissue culture plate (TCP), demonstrating the cell stemness maintenance ability of bioinspired FN-HAMA microcarriers (Fig. 3h).

3.5. *In vitro proangiogenic effect of FN-HAMA@ADSCs*

It is well known that revascularization is a crucial part of the tissue repair and reconstruction process. A tube formation assay was conducted to investigate whether the ADSCs-loaded microcarriers could induce angiogenesis and cell migration. Compared with the ADSCs group, all microcarrier groups exhibited more vital pro-angiogenic ability (Fig. 4a). Notably, HUVEC co-cultured with FN-HAMA@ADSCs demonstrated the most robust tube-forming ability with the highest number of meshes, junctions, and maximum total tube length (Fig. 4b, c, and 4d).

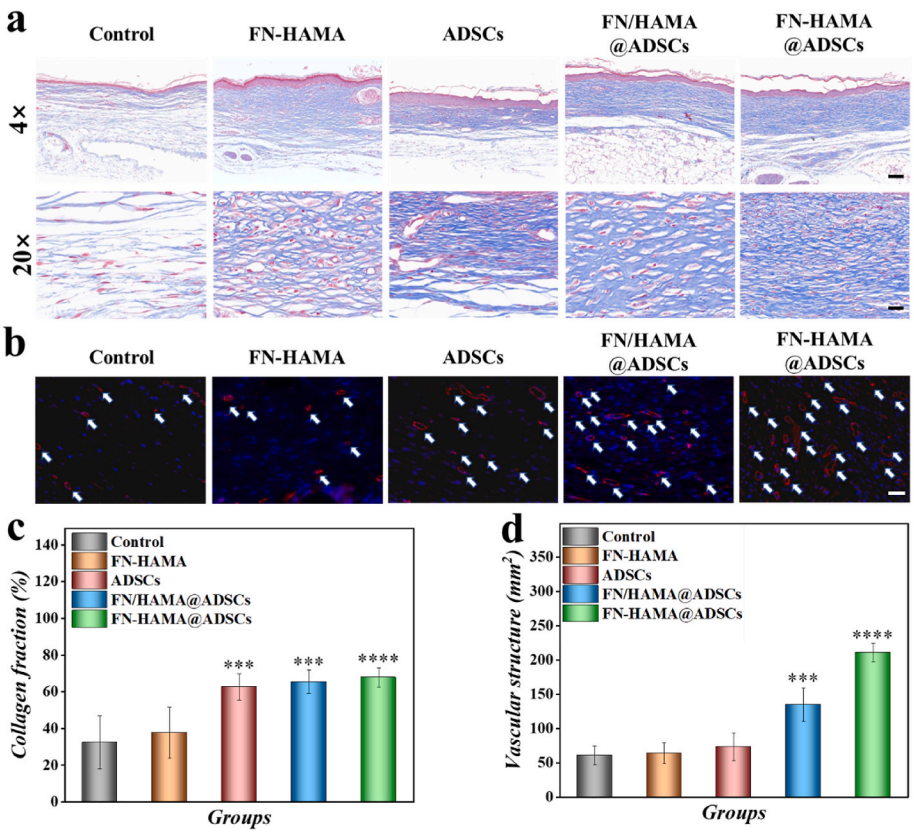

Fig. 6. Effects of collagen deposition and angiogenesis resulted from FN-HAMA@ADSCs. (a) Masson staining images of the diabetic wounds on Day 9 with the treatment of different groups. Scale bar: up: 100 μm; down: 20 μm. (b) Immunofluorescent staining images of CD31 on Day 9 with the treatment of different groups. Blood vessels are labeled with white arrows. Scale bar: 100 μm. (c) Quantitative analysis of collagen positive staining area on day 9. (d) Quantitative analysis of the blood vessel density on day 9. *$p < 0.05$, **$p < 0.01$, ***$p < 0.001$, ****$p < 0.0001$, not significant (ns).

To further investigate the intrinsic mechanism of pro-angiogenesis induced by FN-HAMA@ADSCs, we performed PCR experiments to detect the relative expression of the genes related to angiogenesis, including HIF-1, FGF2, VEGF, and Ang-1. Notably, the relative expression of these genes was considerably up-regulated post encapsulation in FN-HAMA microcarriers, indicating the signaling modulation function of the stem niche-like microenvironments (Fig. 4e). ELISA assays were further performed to measure the supernatant levels of growth factors. The results showed that FN-HAMA@ADSCs could stably produce and release the highest levels of VEGF, HGF, and FGF2 compared to ADSCs and FN/HAMA@ADSCs (Fig. 4f), contributing to the enhanced pro-regenerative and angiogenesis function.

3.6. Promoted diabetic wound repaired in vivo by FN-HAMA@ADSCs

As the favorable biocompatibility and angiogenesis promotion ability of FN-HAMA@ADSCs microcarriers were well established, a mouse type I diabetic wound model was used in this study to further validate their therapeutic effects in vivo. As schemed in Fig. 5a, all mice were induced into hyperglycemic status by intraperitoneal injection of Streptozocin, followed by the fabrication of 8 mm diameter wounds on the back bilaterally. Then, these mice were distributed into five groups and given treatment with PBS, blank FN-HAMA microcarriers, ADSCs, FN/HAMA@ADSCs, and FN-HAMA@ADSCs, respectively. During the healing process, the wound area was monitored every 3 days. Generally, the diabetic trauma was in a chronic inflammatory state with impaired healing due to microangiopathy and neuropathy. It was evident that the FN-HAMA@ADSCs group showed a significantly faster regeneration rate compared to the ADSCs group with direct injection, implying the critical role of microcarriers as a physical barrier for transplanted stem cells. Moreover, the FN-HAMA@ADSCs group outperformed the FN/HAMA@ADSCs group due to their closer stem cell niche-mimicking environment (Fig. 5b,c,5g), corresponding well with in vitro results.

To evaluate the in vivo cell distribution, we delivered the mCherry-labeled ADSCs to the wounds and tracked them using in vivo image system. It was shown that the fluorescence signal could be detected in all the groups, suggesting the existence of ADSCs after 72 h of treatment. In addition, the FN-HAMA@ADSCs group show the slowest decay of fluorescence intensity, indicating the enhanced cell engraftment achieved by FN-HAMA microcarriers (Fig. S10).

The repair of the diabetic wounds was further evaluated by hematoxylin-eosin (H&E) staining (Fig. 5d, S11). A poor tissue reconstruction occurred in PBS and microcapsule treated groups, as demonstrated by the thin skin thickness and the absence of significant hair follicle rejuvenation. Directly injected ADSCs slightly improved the healing process with an increase in skin thickness, revealing the potential pro-regenerative capability of ADSCs. In consistency with the wound area tracing analysis, FN-HAMA@ADSCs treated group showed considerably enhanced dermal thickness (Fig. 5e) and apparent follicular rejuvenation (Fig. 5f) due the simultaneous presence of ADSCs and FN anchoring microcarriers, revealing their practical value in facilitating tissue reconstruction.

To explore the mechanism of the ameliorated wound healing with FN-HAMA@ADSCs treatment, we performed Masson staining to evaluate the collagen deposition in the wound bed (Fig. 6a and c). Increased collagen synthesis along with directional alignment was observed in FN-HAMA@ADSCs treated group, reflecting the improved ECM remodeling, which is crucial for accelerated wound healing. Notably, although dense color was observed in the ADSCs group, the college bundles were sparsely and disorderly distributed, indicating poor tissue reconstruction. Furthermore, angiogenesis of wound tissue was assessed by immunofluorescent staining of CD31 (Fig. 6b). It was shown that the number and density of neovasculature labeled with CD31 were notably increased in the FN-HAMA@ADSCs treated groups, suggesting the angiogenesis effects aroused from the abundant growth factor produced by ADSCs (Fig. 6d). Also, no toxicity from all applied materials was observed in treated mice (Fig. S12). Taken together, the stem cell niche mimic FN-HAMA@ADSCs microcapsule could significantly improve

tissue proliferation and regeneration by enhancing angiogenesis and collagen deposition, thus accelerating diabetic wound healing.

4. Conclusions

Stem cell niches are specific microenvironments inhabited by stem cells, and providing a microenvironment similar to the stem cell niche for transplanted stem cells is expected to enhance cell viability and promote therapeutic efficacy. FN is one of the functional proteins of stem cell niches, responsible for regulating cell adhesion and stemness. In this study, we have developed a natural stem cell niche-inspired microcarrier based on HAMA-conjugated FN with encapsulation of therapeutic ADSCs for diabetic wound healing. HAMA hydrogel possessed excellent water retention and biocompatibility, and the chemically anchored FN in the hydrogel network reproduced the regulatory functions of stem cell niches, therefore improving the cell adhension and viability and maintaining the cell stemness of ADSCs after preculture. In addition, the FN-HAMA microcarriers showed extraordinary regulatory effects on ADSCs to produce multiple growth and paracrine factors (e.g., VEGF, HGF, FGF2), therefore facilitating the migration and angiogenesis of HUVECs. More importantly, an accelerated diabetic wound healing process with promoted neovascularization, follicular rejuvenation, and collagen deposition was achieved using the FN-HAMA microcarriers. Therefore, the stem cell niche-inspired FN-HAMA@ADSCs microcarriers could offer a new way to deliver stem cells while keeping their stemness. This could be useful for hard-healing diabetic wound healing and for a wide range of regenerative medicines.

Ethics approval

All animal experiments were approved by the Animal Investigation Ethics Committee of Nanjing Drum Tower Hospital and performed in accordance with ethical guidelines. The approval number issued by the Laboratory Animal Welfare Ethics Committee of Drum Tower Hospital was 2020AE01109.

CRediT authorship contribution statement

Xiangyi Wu: Investigation, Methodology, Validation, Writing – original draft, Writing – review & editing. **Haofang Zhu:** Investigation, Methodology, Validation. **Junyi Che:** Investigation, Methodology. **Ye Xu:** Supervision, Writing – review & editing. **Qian Tan:** Supervision, Writing – review & editing, Funding acquisition. **Yuanjin Zhao:** Conceptualization, Project administration, Supervision, Funding acquisition.

Declaration of competing interest

The authors declare that they have no known competing financial interests or personal relationships that could have appeared to influence the work reported in this paper.

Acknowledgments

This work was supported by the National Key Research and Development Program of China (2020YFA0908200), the National Natural Science Foundation of China (81974288, T2225003 and 52073060), the Strategic Priority Research Program of the Chinese Academy of Science (XDA16021103), the Guangdong Basic and Applied Basic Research Foundation (2021B1515120054), and the Shenzhen Fundamental Research Program (JCYJ20190813152616459 and JCYJ20210324133214038).

Appendix A. Supplementary data

Supplementary data to this article can be found online at https://doi.org/10.1016/j.bioactmat.2023.02.031.

References

[1] S.B. Xu, L.N. Chang, Y.A. Hu, X.J. Zhao, S.C. Huang, Z.H. Chen, X.L. Ren, X.F. Mei, Tea polyphenol modified, photothermal responsive and ROS generative black phosphorus quantum dots as nanoplatforms for promoting MRSA infected wounds healing in diabetic rats, J. Nanobiotechnol. 19 (1) (2021), https://doi.org/10.1186/s12951-021-01106-w.

[2] X. Zhao, L. Chang, Y. Hu, S. Xu, Z. Liang, X. Ren, X. Mei, Z. Chen, Preparation of photocatalytic and antibacterial MOF nanozyme used for infected diabetic wound healing, ACS Appl. Mater. Interfaces 14 (16) (2022) 18194–18208, https://doi.org/10.1021/acsami.2c03001.

[3] P.A. Shiekh, A. Singh, A. Kumar, Exosome laden oxygen releasing antioxidant and antibacterial cryogel wound dressing OxOBand alleviate diabetic and infectious wound healing, Biomaterials 249 (2020), https://doi.org/10.1016/j.biomaterials.2020.120020.

[4] N.C. Schaper, J.J. van Netten, J. Apelqvist, S.A. Bus, R.J. Hinchliffe, B.A. Lipsky, I. E. Board, Practical Guidelines on the prevention and management of diabetic foot disease (IWGDF 2019 update), Diabetes Metab Res Rev 36 (Suppl 1) (2020), e3266, https://doi.org/10.1002/dmrr.3266.

[5] J. Ouyang, X. Ji, X. Zhang, C. Feng, Z. Tang, N. Kong, A. Xie, J. Wang, X. Sui, L. Deng, Y. Liu, J.S. Kim, Y. Cao, W. Tao, In situ sprayed NIR-responsive, analgesic black phosphorus-based gel for diabetic ulcer treatment, Proc. Natl. Acad. Sci. U. S. A. 117 (46) (2020) 28667–28677, https://doi.org/10.1073/pnas.2016268117.

[6] Y. Liu, J. Fan, M. Lv, K. She, J. Sun, Q. Lu, C. Han, S. Ding, S. Zhao, G. Wang, Y. Zhang, G. Zang, Photocrosslinking silver nanoparticles-aloe vera-silk fibroin composite hydrogel for treatment of full-thickness cutaneous wounds, Regenerative Biomaterials 8 (6) (2021), https://doi.org/10.1093/rb/rbab048.

[7] L. Jin, X. Guo, D. Gao, C. Wu, B. Hu, G. Tan, N. Du, X. Cai, Z. Yang, X. Zhang, NIR-responsive MXene nanobelts for wound healing, NPG Asia Mater. 13 (1) (2021), https://doi.org/10.1038/s41427-021-00289-w.

[8] H.N. Wilkinson, M.J. Hardman, Wound healing: cellular mechanisms and pathological outcomes, Open Biology 10 (9) (2020), https://doi.org/10.1098/rsob.200223.

[9] S.Q. Wang, H. Zheng, L. Zhou, F. Cheng, Z. Liu, H.P. Zhang, L.L. Wang, Q.Y. Zhang, Nanoenzyme-reinforced injectable hydrogel for healing diabetic wounds infected with multidrug resistant bacteria, Nano Lett. 20 (7) (2020) 5149–5158, https://doi.org/10.1021/acs.nanolett.0c01371.

[10] A.O. Lukomskyj, N. Rao, L. Yan, J.S. Pye, H.Y. Li, B. Wang, J.J. Li, Stem cell-based tissue engineering for the treatment of burn wounds: a systematic review of preclinical studies, Stem Cell Reviews and Reports 18 (6) (2022) 1926–1955, https://doi.org/10.1007/s12015-022-10341-z.

[11] L. Shukla, Y.N. Yuan, R. Shayan, D.W. Greening, T. Karnezis, Fat therapeutics: the clinical capacity of adipose-derived stem cells and exosomes for human disease and tissue regeneration, Front. Pharmacol. 11 (2020), https://doi.org/10.3389/fphar.2020.00158.

[12] J.X. Zhang, Y.Z. Liu, Y.T. Chen, L. Yuan, H. Liu, J.C. Wang, Q.R. Liu, Y. Zhang, Adipose-derived stem cells: current applications and future directions in the regeneration of multiple tissues, Stem Cell. Int. 2020 (2020), https://doi.org/10.1155/2020/8810813.

[13] N. Zeng, H.B. Chen, Y.P. Wu, Z.M. Liu, Adipose stem cell-based treatments for wound healing, Front. Cell Dev. Biol. 9 (2022), https://doi.org/10.3389/fcell.2021.821652.

[14] S. Tyeb, P.A. Shiekh, V. Verma, A. Kumar, Adipose-derived stem cells (ADSCs) loaded gelatin-sericin-laminin cryogels for tissue regeneration in diabetic wounds, Biomacromolecules 21 (2) (2020) 294–304, https://doi.org/10.1021/acs.biomac.9b01355.

[15] J.A. Ankrum, J.F. Ong, J.M. Karp, Mesenchymal stem cells: immune evasive, not immune privileged, Nat. Biotechnol. 32 (3) (2014) 252–260, https://doi.org/10.1038/nbt.2816.

[16] J. Galipeau, L. Sensebe, Mesenchymal stromal cells: clinical challenges and therapeutic opportunities, Cell Stem Cell 22 (6) (2018) 824–833, https://doi.org/10.1016/j.stem.2018.05.004.

[17] N. Li, A. Zhan, Y. Jiang, H. Liu, A novel matrix metalloproteinases-cleavable hydrogel loading deferoxamine accelerates diabetic wound healing, Int. J. Biol. Macromol. 222 (Pt A) (2022) 1551–1559, https://doi.org/10.1016/j.ijbiomac.2022.09.185.

[18] C.-C. Zhao, L. Zhu, Z. Wu, R. Yang, N. Xu, L. Liang, Resveratrol-loaded peptide-hydrogels inhibit scar formation in wound healing through suppressing inflammation, Regenerative Biomaterials 7 (1) (2020) 99–108, https://doi.org/10.1093/rb/rbz041.

[19] X. Ren, Y. Hu, L. Chang, S. Xu, X. Mei, Z. Chen, Electrospinning of antibacterial and anti-inflammatory Ag@hesperidin core-shell nanoparticles into nanofibers used for promoting infected wound healing, Regenerative Biomaterials 9 (2022), https://doi.org/10.1093/rb/rbac012.

[20] G. Chen, L. He, P. Zhang, J. Zhang, X. Mei, D. Wang, Y. Zhang, X. Ren, Z. Chen, Encapsulation of green tea polyphenol nanospheres in PVA/alginate hydrogel for promoting wound healing of diabetic rats by regulating PI3K/AKT pathway, Materials Science & Engineering C-Materials for Biological Applications 110 (2020), https://doi.org/10.1016/j.msec.2020.110686.

[21] W.H. Yuan, H.X. Wang, C. Fang, Y.K. Yang, X.Y. Xia, B.G. Yang, Y. Lin, G. Li, L. M. Bian, Microscopic local stiffening in a supramolecular hydrogel network expedites stem cell mechanosensing in 3D and bone regeneration, Mater. Horiz. 8 (6) (2021) 1722–1734, https://doi.org/10.1039/d1mh00244a.

[22] Q. Xu, A. Sigen, Y. Gao, L. Guo, J. Creagh-Flynn, D. Zhou, U. Greiser, Y. Dong, F. Wang, H. Tai, W. Liu, W. Wang, W. Wang, A hybrid injectable hydrogel from hyperbranched PEG macromer as a stem cell delivery and retention platform for diabetic wound healing, Acta Biomater. 75 (2018) 63–74, https://doi.org/10.1016/j.actbio.2018.05.039.

[23] Y.P. Liang, J.H. He, B.L. Guo, Functional hydrogels as wound dressing to enhance wound healing, ACS Nano 15 (8) (2021) 12687–12722, https://doi.org/10.1021/acsnano.1c04206.

[24] A.C. Daly, L. Riley, T. Segura, J.A. Burdick, Hydrogel microparticles for biomedical applications, Nat. Rev. Mater. 5 (1) (2020) 20–43, https://doi.org/10.1038/s41578-019-0148-6.

[25] J.M. Unagolla, A.C. Jayasuriya, Hydrogel-based 3D bioprinting: a comprehensive review on cell-laden hydrogels, bioink formulations, and future perspectives, Appl. Mater. Today 18 (2020), https://doi.org/10.1016/j.apmt.2019.100479.

[26] J.Z. Wu, G. Li, T.J. Ye, G.H. Lu, R.M. Li, L.F. Deng, L. Wang, M. Cai, W.G. Cui, Stem cell-laden injectable hydrogel microspheres for cancellous bone regeneration, Chem. Eng. J. 393 (2020), https://doi.org/10.1016/j.cej.2020.124715.

[27] L. Lukjanenko, M.J. Jung, N. Hegde, C. Perruisseau-Carrier, E. Migliavacca, M. Rozo, S. Karaz, G. Jacot, M. Schmidt, L.J. Li, S. Metairon, F. Raymond, U. Lee, F. Sizzano, D.H. Wilson, N.A. Dumont, A. Palini, R. Fassler, P. Steiner, P. Descombes, M.A. Rudnicki, C.M. Fan, J. von Maltzahn, J.N. Feige, C. F. Bentzinger, Loss of fibronectin from the aged stem cell niche affects the regenerative capacity of skeletal muscle in mice, Nat. Med. 22 (8) (2016) 897, https://doi.org/10.1038/nm.4126.

[28] Y. Li, J. Wang, D.J. Qian, L. Chen, X.M. Mo, L. Wang, Y. Wang, W.G. Cui, Electrospun fibrous sponge via short fiber for mimicking 3D ECM, J. Nanobiotechnol. 19 (1) (2021), https://doi.org/10.1186/s12951-021-00878-5.

[29] W.J. Liu, Z. Zhong, N. Hu, Y.X. Zhou, L. Maggio, A.K. Miri, A. Fragasso, X.Y. Jin, A. Khademhosseini, Y.S. Zhang, Coaxial extrusion bioprinting of 3D microfibrous constructs with cell-favorable gelatin methacryloyl microenvironments, Biofabrication 10 (2) (2018), https://doi.org/10.1088/1758-5090/aa9d44.

[30] S. Lee, A.E. Stanton, X. Tong, F. Yang, Hydrogels with enhanced protein conjugation efficiency reveal stiffness-induced YAP localization in stem cells depends on biochemical cues, Biomaterials 202 (2019) 26–34, https://doi.org/10.1016/j.biomaterials.2019.02.021.

[31] A.E. Stanton, X. Tong, S. Lee, F. Yang, Biochemical ligand density regulates yes-associated protein translocation in stem cells through cytoskeletal tension and integrins, ACS Appl. Mater. Interfaces 11 (9) (2019) 8849–8857, https://doi.org/10.1021/acsami.8b21270.

[32] A.E. Stanton, X. Tong, F. Yang, Extracellular matrix type modulates mechanotransduction of stem cells, Acta Biomater. 96 (2019) 310–320, https://doi.org/10.1016/j.actbio.2019.06.048.

[33] B.G. Yang, K.C. Wei, C. Loebel, K.Y. Zhang, Q. Feng, R. Li, S.H.D. Wong, X.Y. Xu, C. H. Lau, X.Y. Chen, P.C. Zhao, C. Yin, J.A. Burdick, Y. Wang, L.M. Bian, Enhanced mechanosensing of cells in synthetic 3D matrix with controlled biophysical dynamics, Nat. Commun. 12 (1) (2021), https://doi.org/10.1038/s41467-021-23120-0.

[34] J.L. Yang, Y. Han, J.W. Lin, Y. Zhu, F. Wang, L.F. Deng, H.Y. Zhang, X.Y. Xu, W. G. Cui, Ball-bearing-inspired polyampholyte-modified microspheres as bio-lubricants attenuate osteoarthritis, Small 16 (44) (2020), https://doi.org/10.1002/smll.202004519.

[35] Y. Man, M.J. Ban, A. Li, X.X. Jin, Y.F. Du, L.G. Pan, A microfluidic colorimetric biosensor for in-field detection of Salmonella in fresh-cut vegetables using thiolated polystyrene microspheres, hose-based microvalve and smartphone imaging APP, Food Chem. 354 (2021), https://doi.org/10.1016/j.foodchem.2021.129578.

[36] H. Zhang, L.Z. Hao, J.A. Pan, Q. Gao, J.F. Zhang, R.K. Kankala, S.B. Wang, A. Z. Chen, H.L. Zhang, Microfluidic fabrication of inhalable large porous microspheres loaded with H2S-releasing aspirin derivative for pulmonary arterial hypertension therapy, J. Contr. Release 329 (2021) 286–298, https://doi.org/10.1016/j.jconrel.2020.11.060.

[37] Z.Y. Zhao, G. Li, H.T. Ruan, K.Y. Chen, Z.W. Cai, G.H. Lu, R.M. Li, L.F. Deng, M. Cai, W.G. Cui, Capturing magnesium ions via microfluidic hydrogel microspheres for promoting cancellous bone regeneration, ACS Nano 15 (8) (2021) 13041–13054, https://doi.org/10.1021/acsnano.1c02147.

[38] Y.Q. Li, W. Liu, F. Liu, Y. Zeng, S.M. Zuo, S.Y. Feng, C.X. Qi, B.J. Wang, X.J. Yan, A. Khademhosseini, J. Bai, Y.A. Du, Primed 3D injectable microniches enabling low-dosage cell therapy for critical limb ischemia, Proc. Natl. Acad. Sci. U.S.A 111 (37) (2014) 13511–13516, https://doi.org/10.1073/pnas.1411295111.

[39] G.P. Chen, F.Y. Wang, M. Nie, H. Zhang, H. Zhang, Y.J. Zhao, Roe-inspired stem cell microcapsules for inflammatory bowel disease treatment, Proc. Natl. Acad. Sci. U.S.A 118 (43) (2021), https://doi.org/10.1073/pnas.2112704118j1of8.

[40] S. Trujillo, C. Gonzalez-Garcia, P. Rico, A. Reid, J. Windmill, M.J. Dalby, M. Salmeron-Sanchez, Engineered 3D hydrogels with full-length fibronectin that sequester and present growth factors, Biomaterials 252 (2020), https://doi.org/10.1016/j.biomaterials.2020.120104.

[41] A.B. Bello, D. Kim, D. Kim, H. Park, S.H. Lee, Engineering and functionalization of gelatin biomaterials: from cell culture to medical applications, Tissue Eng. B Rev. 26 (2) (2020) 164–180, https://doi.org/10.1089/ten.teb.2019.0256.

[42] H. Xing, H. Lee, L.J. Luo, T.R. Kyriakides, Extracellular matrix-derived biomaterials in engineering cell function, Biotechnol. Adv. 42 (2020), https://doi.org/10.1016/j.biotechadv.2019.107421.

[43] J.J. Xue, T. Wu, J.C. Qiu, S. Rutledge, M.L. Tanes, Y.N. Xia, Promoting cell migration and neurite extension along uniaxially aligned nanofibers with biomacromolecular particles in a density gradient, Adv. Funct. Mater. 30 (40) (2020), https://doi.org/10.1002/adfm.202002031.

[44] M.T. Tierney, A. Gromova, F.B. Sesillo, D. Sala, C. Spenle, G. Orend, A. Sacco, Autonomous extracellular matrix remodeling controls a progressive adaptation in muscle stem cell regenerative capacity during development, Cell Rep. 14 (8) (2016) 1940–1952, https://doi.org/10.1016/j.celrep.2016.01.072.

[45] Y. Kong, B. Ma, F. Liu, D. Chen, S. Zhang, J. Duan, Y. Huang, Y. Sang, J. Wang, D. Li, H. Liu, S. Wang, Cellular stemness maintenance of human adipose-derived stem cells on ZnO nanorod arrays, Small 15 (51) (2019), https://doi.org/10.1002/smll.201904099.

[46] Y. Zhou, C. Liu, J. He, L. Dong, H. Zhu, B. Zhang, X. Feng, W. Weng, K. Cheng, M. Yu, H. Wang, KLF2(+) stemness maintains human mesenchymal stem cells in bone regeneration, Stem Cell. 38 (3) (2020) 395–409, https://doi.org/10.1002/stem.3120.